

Journal of Biomedical Optics

SPIEDigitalLibrary.org/jbo

Linear-array-based photoacoustic imaging of human microcirculation with a range of high frequency transducer probes

Haroon Zafar
Aedán Breathnach
Hrebesh M. Subhash
Martin J. Leahy

Linear-array-based photoacoustic imaging of human microcirculation with a range of high frequency transducer probes

Haroon Zafar,^{a,b} Aedán Breathnach,^{a,b} Hrebesh M. Subhash,^{a,b} and Martin J. Leahy^{a,b,c,*}

^aNational University of Ireland Galway, School of Physics, Tissue Optics and Microcirculation Imaging Facility, Arts and Science Building, University Road, Galway, Ireland

^bNational Biophotonics and Imaging Platform, Research Office, 121 St. Stephens Green, Dublin 2, Ireland

^cRoyal College of Surgeons in Ireland, 121 St. Stephens Green, Dublin 2, Ireland

Abstract. Photoacoustic imaging (PAI) with a linear-array-based probe can provide a convenient means of imaging the human microcirculation within its native structural context and adds functional information. PAI using a multielement linear transducer array combined with multichannel collecting system was used for *in vivo* volumetric imaging of the blood microcirculation, the total concentration of hemoglobin (HbT), and the hemoglobin oxygen saturation (sO₂) within human tissue. Three-dimensional (3-D) PA and ultrasound (US) volumetric scans were acquired from the forearm skin by linearly translating the transducer with a stepper motor over a region of interest, while capturing two-dimensional images using 15, 21, and 40 MHz frequency transducer probes. For the microvasculature imaging, PA images were acquired at 800- and 1064-nm wavelengths. For the HbT and sO₂ estimates, PA images were collected at 750- and 850-nm wavelengths. 3-D microcirculation, HbT, and sO₂ maps of the forearm skin were obtained from normal subjects. The linear-array-based PAI has been found promising in terms of resolution, imaging depth, and imaging speed for *in vivo* microcirculation imaging within human skin. We believe that a reflection type probe, similar to existing clinical US probes, is most likely to succeed in real clinical applications. Its advantages include ease of use, speed, and familiarity for radiographers and clinicians. © 2015 Society of Photo-Optical Instrumentation Engineers (SPIE) [DOI: 10.1117/1.JBO.20.5.051021]

Keywords: microcirculation imaging; photoacoustic; linear-array transducer; high frequency ultrasound.

Paper 140632SSPR received Sep. 30, 2014; accepted for publication Dec. 2, 2014; published online Dec. 23, 2014.

1 Introduction

The microcirculation serves key functions in the body, e.g., regulate blood pressure and body temperature, exchange nutrients and metabolic waste to body, etc. Structural and functional changes within the microcirculation have been associated with various diseases including cancer, diabetes, psoriasis, capillary malformation, and Raynaud's disease.¹⁻⁴ Microcirculation imaging can provide early indication of disease prior to clinical suspicion.⁵ The importance of noninvasive imaging techniques to get a better understanding of the vascular involvement in such diseases is critical. There are various techniques available for *in vivo* imaging of blood vessels within human skin. Capillaroscopy, videocapillaroscopy, laser Doppler perfusion imaging, and dynamic laser speckle imaging are commonly used, but all these techniques are limited to imaging vessels close to the surface of the skin.⁶⁻¹⁰ Optical coherence tomography¹¹ can be combined with novel flow contrast schemes^{12,13} to obtain high resolution microvascular morphology but with a low imaging depth.

Photoacoustic imaging (PAI) breaks through the optical diffusion limit and can provide microvasculature information at a high penetration depth with resolution superior than pure optical techniques by taking advantage of the low acoustic scattering in the tissue. In PAI, image contrast is dominated by the strong optical absorption of hemoglobin; therefore, vasculature can be imaged effectively. In the last few years, there has been a huge interest in the development of PAI techniques with the applications explored

in dermatology,¹⁴ oncology,^{15,16} vascular biology,^{17,18} cardiology,^{19,20} ophthalmology,^{21,22} neurology,²³ and gastroenterology.²⁴ The most commonly used PAI systems employ either a tomographic^{25,26} or planar geometry with a linear transducer array.^{27,28} In conventional photoacoustic tomography (PAT), an entire region of interest is excited using full field illumination and the photoacoustic (PA) waves are simultaneously detected either using single ultrasound (US) detector or an array of detectors. Then an acoustic back propagation algorithm is used to reconstruct a three-dimensional (3-D) image. Linear-array-based PAI systems detect PA waves from limited angles around the object using an array of detectors. PAT systems suffer from low frame rates due to the need for hundreds to thousands of laser pulses per frame. Linear-array-based PAI systems allow images to be acquired with just a few laser pulses and provide much higher frame rates which make them more suitable for clinical imaging applications. A variety of PAI systems have been developed based on various scanning configurations and reconstruction algorithms to get the optimal resolution, imaging depth, and contrast. Although PAT scanners based on spherical and cylindrical detection geometries offer large angular aperture for data collection and an accurate image reconstruction, they are not well suited for imaging highly superficial features such as the skin microvasculature for clinical imaging applications.²⁹ Moreover, the commonly used single element PAI systems cannot satisfy the requirement of real-time data acquisition and imaging, which is a prerequisite in the clinical scenario. Linear-array-

*Address all correspondence to: Martin J. Leahy, E-mail: martin.leahy@nuiagalway.ie

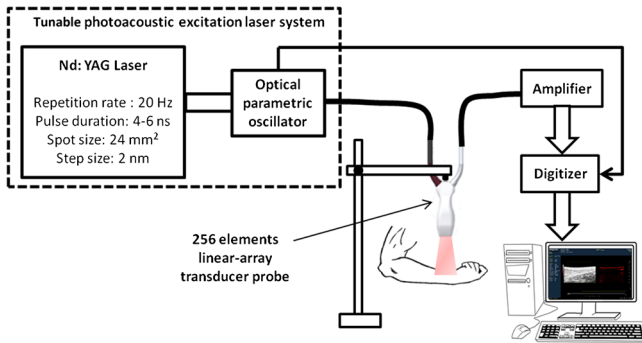


Fig. 1 Schematic of the experimental setup used in this study. Combined photoacoustic (PA) and high-frequency ultrasound (US) imaging within human forearm skin using linear-array transducer probe.

based PAI is an alternative option, particularly for clinical imaging of skin and subcutaneous morphologies. In this study, PAI based on a high-frequency multielement linear-array transducer combined with a multichannel collecting system was used for volumetric structural and functional imaging within human skin. *In vivo* 3-D microcirculation, total concentration of hemoglobin (HbT), and the hemoglobin oxygen saturation (sO_2) maps of the human forearm skin were obtained. The high-frequency linear-array transducer probes used in this study are similar in style, shape, and use to regular hand-held clinical US probes, which can easily be acoustically coupled to the skin and moved around while imaging in real time.

2 Materials and Methods

A schematic of the experimental setup used in this study is shown in Fig. 1. A combined PA and US imaging system were operated with a linear-array transducer probe. The key

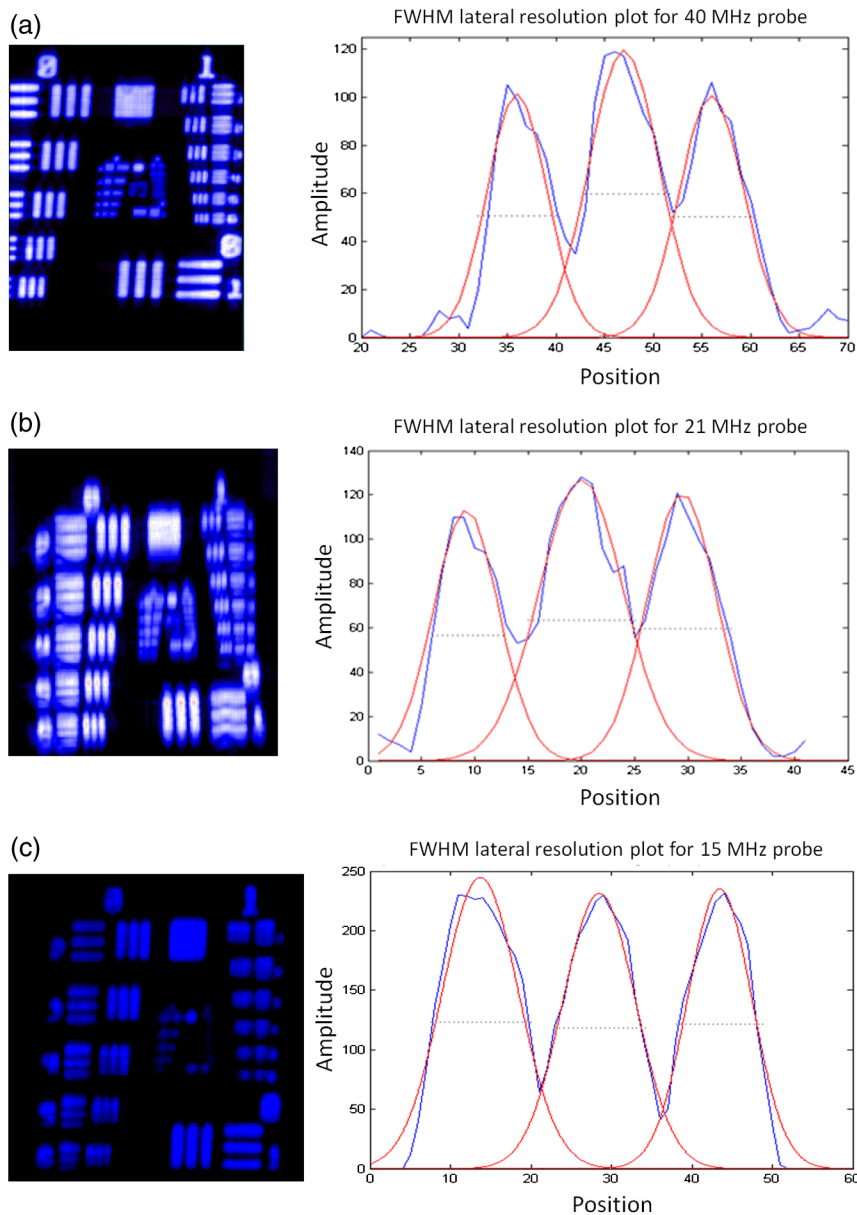


Fig. 2 The maximum intensity projection (MIP) images of the 1951 USAF target scanned by (a) 40 MHz, (b) 21 MHz, and (c) 15 MHz frequency transducer probes along with the intensity profiles and the fitted Gaussian functions.

elements of the PAI system (Vevo LAZR, Fujifilm VisualSonics) are: tunable PA excitation laser system (optical parametric oscillator pumped by frequency-doubled Nd:YAG laser with a repetition rate of 20 Hz, pulse duration of 4 to 6 ns, spot size of 24 mm², and step size of 2 nm), multielement linear-array transducer, amplifier, and a digitizer. Each linear-array transducer probe used in this study consisted of 256 elements, which were divided into four quadrants, each with 64

elements. Pulsed laser light was focused into the tissue through two fiber optic bundles (20 × 1.25 mm) mounted on each side of the acoustic aperture of the transducer probe, emitting two laser beams at an angle of 30 deg relative to the imaging plane. The generated PA waves propagated back to the transducer probe were coupled through US gel and acquired by the transducer array. For each laser pulse, the PA signals were captured by one quadrant of the transducer array. Since four pulses were

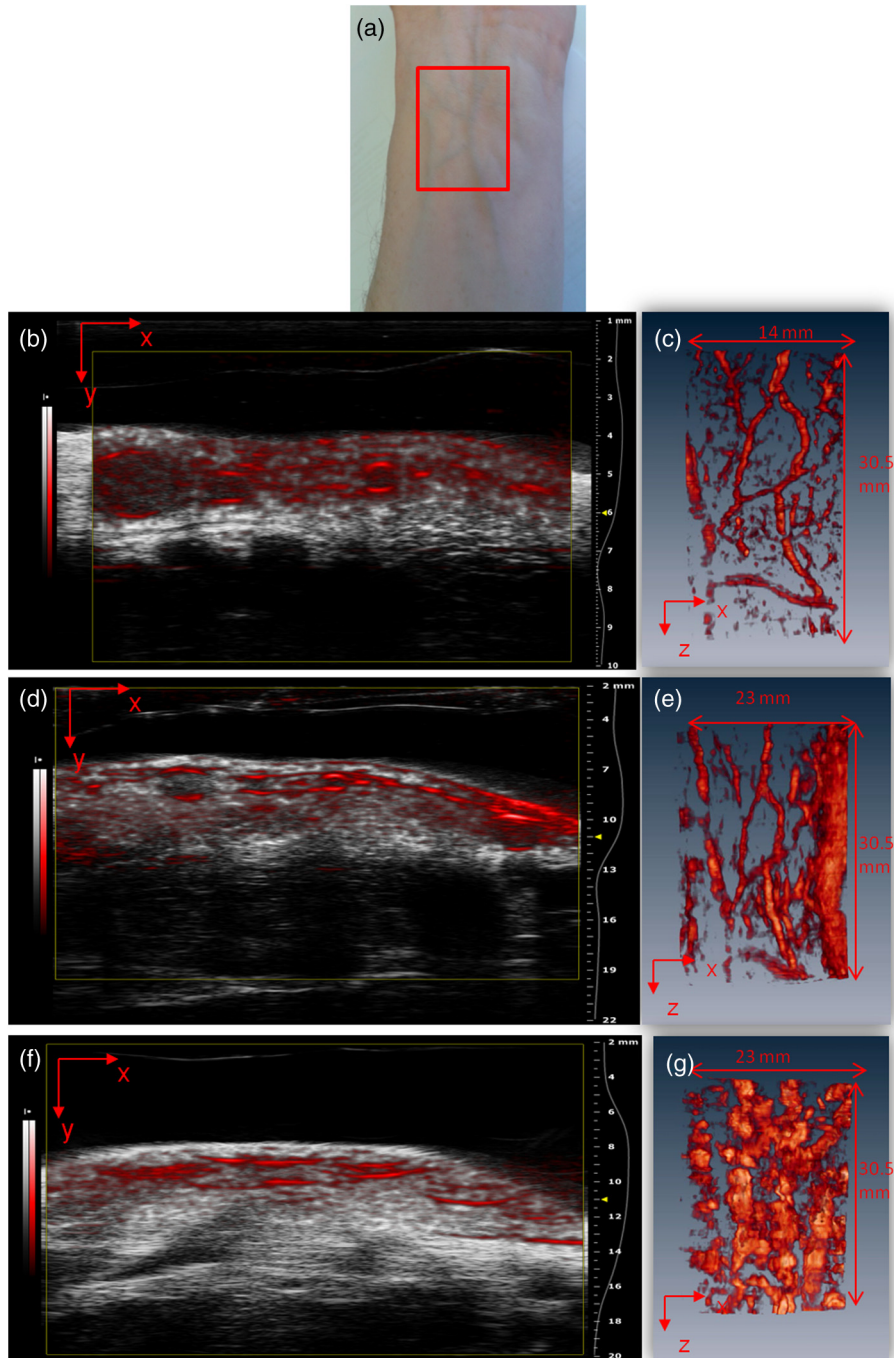


Fig. 3 *In vivo* PA/US images of the human forearm acquired using 40, 21, and 15 MHz frequency transducer probes at 800-nm wavelength: (a) photograph taken from the subject showing the forearm skin examined by PA and high-frequency US imaging (b, d, and f) fused PA/US vertical (x - y) slices (B-scans) of the forearm skin acquired using 40, 21, and 15 MHz frequency transducer probes, respectively (c, e, and g) MIP images through the PA volumes of the human forearm acquired using 40, 21, and 15 MHz frequency transducer probes, respectively.

required for each full width image, the frame rate was one-fourth of the laser repetition rate (i.e., 5 Hz). The PA information was passed onto a computer through an amplifier and a digitizer where it was processed into a 3-D image.

PAI in this work was performed using three transducer probes of center frequencies: 15, 21, and 40 MHz. The

15 MHz probe (broadband frequency: 9 to 18 MHz) provides an axial resolution of $100\ \mu\text{m}$, imaging depth up to 36 mm, and imaging width up to 32 mm. The 21 MHz probe (broadband frequency: 13 to 24 MHz) provides an axial resolution of $75\ \mu\text{m}$, imaging depth up to 20 mm, and imaging width up to 23 mm. The 40 MHz probe (broadband frequency: 32 to 55 MHz)

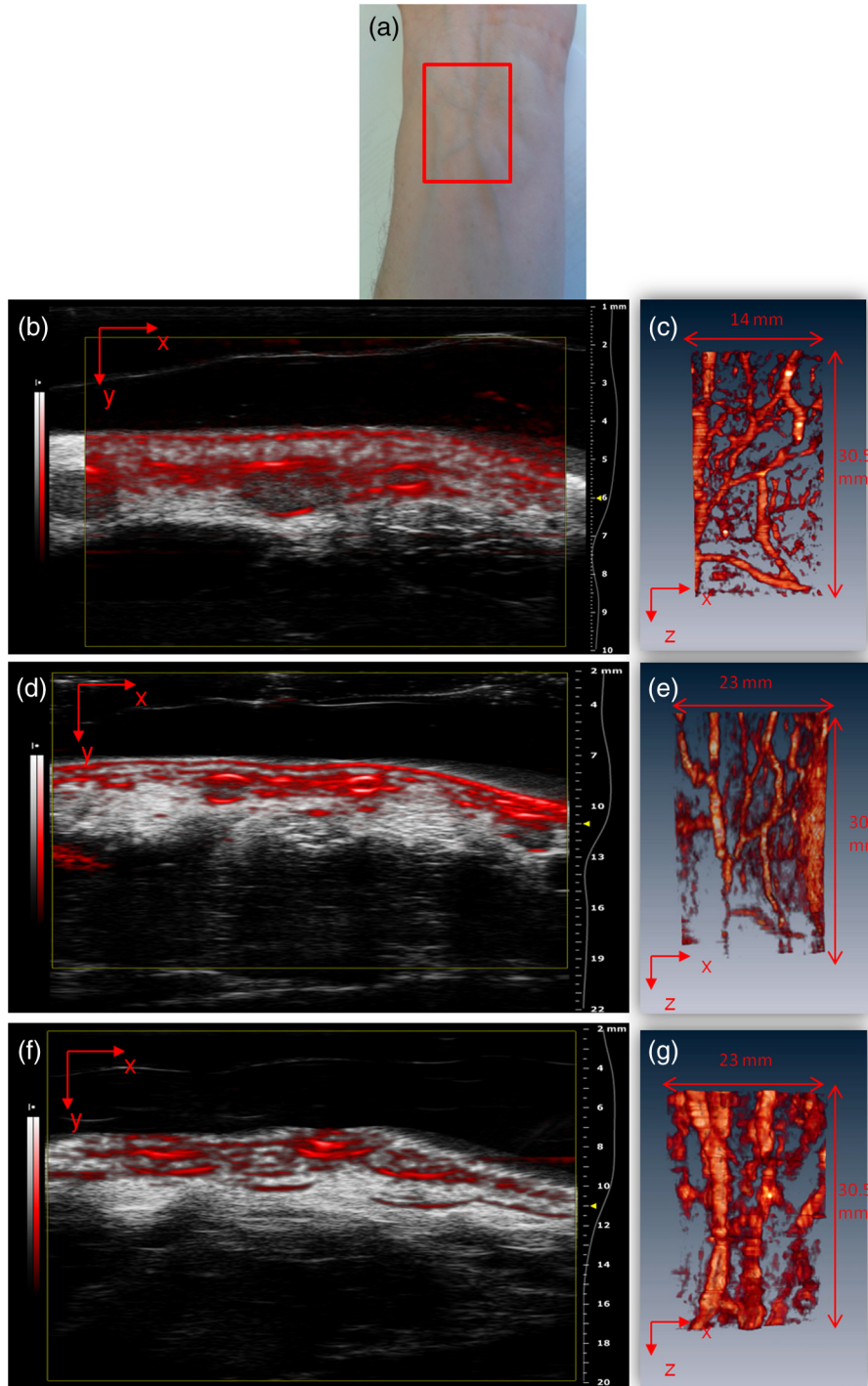


Fig. 4 *In vivo* PA/US images of the human forearm acquired using 40, 21, and 15 MHz frequency transducer probes at 1064-nm wavelength: (a) photograph taken from the subject showing the forearm skin examined by PA and high-frequency US imaging (b, d, and f) fused PA/US vertical (x - y) slices (B-scans) of the forearm skin acquired using 40, 21, and 15 MHz frequency transducer probes, respectively (c, e, and g) MIP images through the PA volumes of the human forearm acquired using 40, 21, and 15 MHz frequency transducer probes, respectively.

provides an axial resolution of $40\ \mu\text{m}$, imaging depth up to 15 mm, and imaging width up to 14.1 mm. The lateral resolution of each transducer probe was measured by scanning a 1951 United States Air Force (USAF) resolution test standard and determining the largest pattern that cannot be discerned. Figures 2(a)–2(c) show the maximum intensity projection (MIP) images of the 1951 USAF target scanned by 40, 21, and 15 MHz frequency transducer probes, respectively, along with the intensity profiles and the fitted Gaussian functions. The full width at half maximum lateral resolutions for 15, 21, and 40 MHz frequency transducer probes were found to be 314, 158, and $140\ \mu\text{m}$, respectively.

This study was approved by National University of Ireland, Galway Research Ethics Committee and written informed consent was obtained from the volunteers. All the experimental procedures were in accordance with the Helsinki declaration of 1975, as revised in 2008. *In vivo* images of the subcutaneous vasculature in the human forearm were acquired using 15, 21, and 40 MHz frequency transducer probes. The forearm skin was acoustically coupled to the transducer probe head

through US gel and successive PA and US scans were acquired. 3-D data sets were collected by linearly translating the transducer (with integrated optical fibers) with a stepper motor over a region of interest, while capturing each two-dimensional (2-D) image of the 3-D stack. For a single 3-D PA/US scan, 300 frames (B-scans) were acquired over a region of 30 mm with a step size of 0.1 mm. The data acquisition time was 60 s.

3 Results and Discussion

Figure 3 shows *in vivo* images of the human forearm acquired using 40, 21, and 15 MHz frequency transducer probes at 800-nm wavelength. The fluence was below the safe maximum permissible exposure of $20\ \text{mJ}/\text{cm}^2$ for human skin.³⁰ The 800-nm wavelength was used to obtain sufficient tissue penetration depth because of the lowest light absorbance in the tissue components such as melanin, oxy- and deoxyhemoglobin, and lipid and water in the near-infrared (NIR) wavelength range (600 to 1000 nm). The photograph taken from the subject showing the forearm skin examined by PA/US is shown in Fig. 3(a).

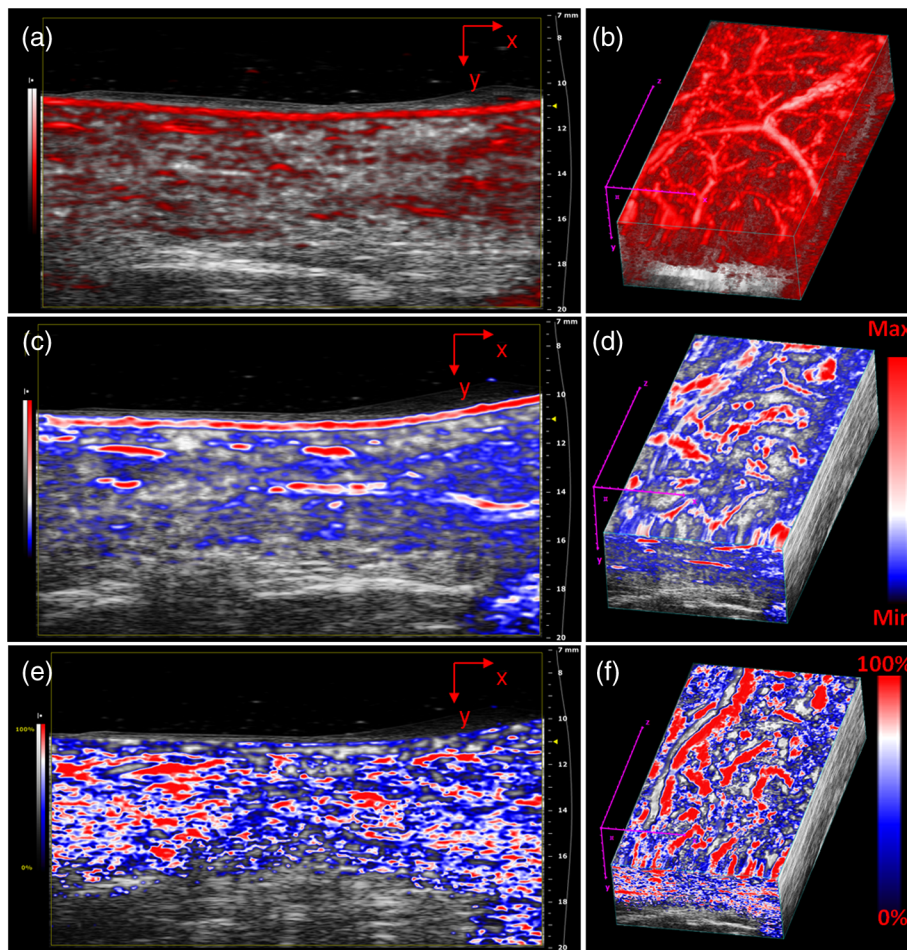


Fig. 5 *In vivo* coregistered PA and ultrasound (HFUS) images of the human forearm acquired using 21 MHz frequency transducer probe: (a) fused PA and US vertical (x - y) slice (B-scan) of the forearm skin for a $22 \times 20\ \text{mm}^2$ region acquired at 800-nm wavelength. (b) Volume rendered representation of the coregistered PA and US data of the forearm skin for a $40 \times 22 \times 20\ \text{mm}^3$ region acquired at 800-nm wavelength. (c) Fused PA (HbT) and US B-scan of the forearm skin for a $23 \times 20\ \text{mm}^2$ region acquired at 750- and 850-nm wavelengths. (d) Volume rendered representation of the coregistered PA (HbT) and US data of the forearm skin for a $40 \times 23 \times 20\ \text{mm}^3$ region acquired at 750- and 850-nm wavelengths. (e) Fused PA ($s\text{O}_2$) and US B-scan of the forearm skin for a $23 \times 20\ \text{mm}^2$ region acquired at 750- and 850-nm wavelengths. (f) Volume rendered representation of the coregistered PA ($s\text{O}_2$) and US data of the forearm skin for a $40 \times 23 \times 20\ \text{mm}^3$ region acquired at 750- and 850-nm wavelengths.

Figures 3(b), 3(d), and 3(f) show fused PA/US single vertical (x - y) slices (B-scans) of the forearm skin acquired using 40, 21, and 15 MHz frequency transducer probes, respectively. The US image (gray scale) shows the layered skin morphology. The PA data (red) shows several blood vessels distributed throughout the dermis and the underlying subcutaneous tissue. Figures 3(c), 3(e), and 3(g) show MIP images through the PA volumes obtained using 40, 21, and 15 MHz frequency transducer probes, respectively. These figures demonstrate the ability of the system to detect the PA signal from the microvasculature as a series of 2-D images rendered in 3-D. High imaging depths can be achieved using low frequency transducer probes but with a lower resolution, as a tradeoff, due to the decreasing attenuation of US with frequency. Although the ultimate resolution limit is defined by acoustic attenuation, other factors such as element size, detector bandwidth, and aperture can be limiting factors in practice.

Figure 4 shows *in vivo* images of the human forearm acquired using 40, 21, and 15 MHz frequency transducer probes at a 1064-nm wavelength. The fluence was once again below the safe maximum permissible exposure of 20 mJ/cm² for human skin. The photograph taken from the subject showing the forearm skin examined by PA/US is shown in Figure 4(a). Figures 4(b), 4(d), and 4(f) show fused PA/US single vertical (x - y) slices (B-scans) of the forearm skin acquired using 40, 21, and 15 MHz frequency transducer probes, respectively. Figures 4(c), 4(e), and 4(g) show MIP images through the PA volumes obtained using 40, 21, and 15 MHz frequency transducer probes, respectively. The lower optical attenuation by blood at 1064 nm compared to 800 nm resulted in a higher penetration depth than was obtained in Fig. 3.

PAI provides an integrated platform for structural and functional imaging by combining high contrast and spectroscopic-based specificity of optical imaging with high spatial resolution of US imaging. Figure 5 shows coregistered PA and US images of the human forearm acquired using 21 MHz frequency transducer probe. The acquired scans measured 40 (length) \times 22 (width) \times 20 (depth) mm³. Figure 5(a) shows a B-scan of the fused PA and US image of the forearm skin for a 22 \times 20 mm² region acquired at 800-nm wavelength. Figure 5(b) shows the volume rendered representation of the coregistered PA and US data of the forearm skin for a 40 \times 22 \times 20 mm³ region. The high optical contrast coregistered with high resolution US imaging allows real-time *in vivo* imaging of deep tissues with detailed anatomical analysis. A supporting movie (Fig. 6) is provided to present the rotating structure of the PA volume which illustrates the network of blood vessels that has been detected. Oxygenated hemoglobin (HbO₂) has different absorption characteristics than deoxygenated hemoglobin (Hb) so an estimate of HbT and sO₂ can be derived and displayed as a parametric map by imaging with different wavelengths of light. For the HbT and sO₂ estimates, PA images were collected at 750- and 850-nm wavelengths. Figure 5(c) shows a B-scan of the fused PA (HbT) and US image of the forearm skin for a 22 \times 20 mm² region. Figure 5(d) shows the volume rendered representation of the coregistered PA (HbT) and US data of the forearm skin for a 40 \times 23 \times 20 mm³ region. Figure 5(e) shows a B-scan of the fused PA (sO₂) and US image of the forearm skin for a 22 \times 20 mm² region. Figure 5(f) shows the volume rendered representation of the coregistered PA (sO₂) and US data of the forearm skin for a 40 \times 23 \times 20 mm³ region.

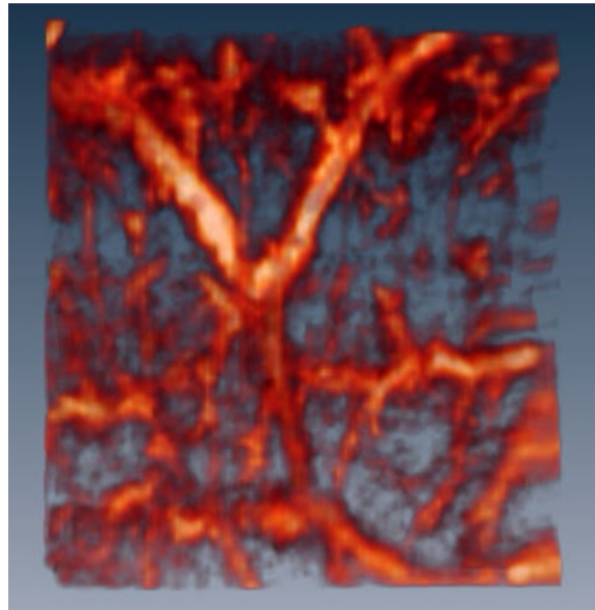


Fig. 6 Rotating structure of the rendered PA volume (Video 1, MPG 4.31 MB) [URL: <http://dx.doi.org/10.1117/1.JBO.20.5.051021.1>].

The linear-array-based PAI has been found promising in terms of resolution, imaging depth, and imaging speed for *in vivo* microcirculation imaging within human skin. However, significant challenges remain, particularly with the imaging depth. The presented results clearly show the feasibility of linear-array-based PAI as a clinical tool for *in vivo* volumetric imaging of the blood microcirculation, HbT, and sO₂ within human tissue. The 3-D microcirculation, HbT, and sO₂ maps obtained will be useful for clinical imaging applications such as management of cancer including screening, diagnosis, treatment planning, therapy monitoring, and accurate measurement of metabolic rate during early diagnosis and treatment of various skin and subcutaneous tissue disorders. We believe that the reflection type probe used in this study is most likely to succeed in real clinical applications. Its advantages include ease of use, speed, and familiarity for radiographers and clinicians.

Acknowledgments

This research was supported by the Science Foundation Ireland (SFI). Haroon Zafar is supported by a Hardiman Fellowship from NUI Galway.

References

1. E. M. Kohner, "Dynamic changes in the microcirculation of diabetics as related to diabetic microangiopathy," *Acta Med. Scand. Suppl.* **578**, 41–47 (1975).
2. J. Folkman, "Proceedings: tumor angiogenesis factor," *Cancer Res.* **34**(8), 2109–2113 (1974).
3. M. Cutolo et al., "Raynaud's phenomenon and the role of capillaroscopy," *Arthritis Rheuma* **48**(11), 3023–3030 (2003).
4. R. H. Bull et al., "Intravital video-capillaroscopy for the study of the microcirculation in psoriasis," *Br. J. Dermatol.* **126**(5), 436–445 (1992).
5. K. Weidlich et al., "Changes in microcirculation as early markers for infection in preterm infants—an observational prospective study," *Pediatr. Res.* **66**(4), 461–465 (2009).
6. P. Humbert et al., "Capillaroscopy and videocapillaroscopy assessment of skin microcirculation: dermatologic and cosmetic approaches," *J. Cosmet. Dermatol.* **4**(3), 153–162 (2005).

7. Z. A. Awan, T. Wester, and K. Kvernebo, "Human microvascular imaging: a review of skin and tongue videomicroscopy techniques and analyzing variables," *Clin. Physiol. Funct. Imaging* **30**(2), 79–88 (2010).
8. K. Murray et al., "Comparison of red and green laser Doppler imaging of blood flow," *Laser Surg. Med.* **35**(3), 191–200 (2004).
9. B. Ruth, J. Schmand, and D. Abendroth, "Noncontact determination of skin blood flow using the laser speckle method: application to patients with peripheral arterial occlusive disease (PAOD) and to type-I diabetics," *Laser Surg. Med.* **13**(2), 179–188 (1993).
10. H. Y. Cheng et al., "Laser speckle imaging of blood flow in microcirculation," *Phys. Med. Biol.* **49**, 1347–1357 (2004).
11. D. Huang et al., "Optical coherence tomography," *Science* **254**, 1178–1181 (1991).
12. R. K. Wang et al., "Three dimensional optical angiography," *Opt. Express* **15**(7), 4083–4097 (2007).
13. H. Zafar et al., "Assessment of psoriatic plaque *in vivo* with correlation mapping optical coherence tomography," *Skin Res. Technol.* **20**(2), 141–146 (2014).
14. E. Z. Zhang et al., "Multimodal photoacoustic and optical coherence tomography scanner using an all optical detection scheme for 3D morphological skin imaging," *Biomed. Opt. Express* **2**, 2202–2215 (2011).
15. S. Mallidi, G. P. Luke, and S. Emelianov, "Photoacoustic imaging in cancer detection, diagnosis and treatment guidance," *Trends Biotechnol.* **29**, 213–221 (2011).
16. J. Yao, K. I. Maslov, and L. V. Wang, "*In vivo* photoacoustic tomography of total blood flow and potential imaging of cancer angiogenesis and hypermetabolism," *Technol. Cancer Res. Treat.* **11**, 301–307 (2012).
17. S. Oladipupo et al., "VEGF is essential for hypoxia-inducible factor-mediated neovascularization but dispensable for endothelial sprouting," *Proc. Natl. Acad. Sci. U.S.A.* **108**, 13264–13269 (2011).
18. S. Oladipupo et al., "Conditional HIF-1 induction produces multistage neovascularization with stage-specific sensitivity to VEGFR inhibitors and myeloid cell independence," *Blood* **117**, 4142–4153 (2011).
19. K. Jansen et al., "Intravascular photoacoustic imaging of human coronary atherosclerosis," *Opt. Lett.* **36**, 597–599 (2011).
20. B. Wang et al., "Plasmonic intravascular photoacoustic imaging for detection of macrophages in atherosclerotic plaques," *Nano Lett.* **9**, 2212–2217 (2009).
21. S. Hu et al., "Label-free photoacoustic ophthalmic angiography," *Opt. Lett.* **35**, 1–3 (2010).
22. S. Jiao et al., "Photoacoustic ophthalmoscopy for *in vivo* retinal imaging," *Opt. Express* **18**, 3967–3972 (2010).
23. S. Hu et al., "Intravital imaging of amyloid plaques in a transgenic mouse model using optical-resolution photoacoustic microscopy," *Opt. Lett.* **34**, 3899–3901 (2009).
24. J. M. Yang et al., "Photoacoustic endoscopy," *Opt. Lett.* **34**, 1591–1593 (2009).
25. C. Li and L. V. Wang, "Photoacoustic tomography and sensing in biomedicine," *Phys. Med. Biol.* **54**, R59–R97 (2009).
26. V. W. Lihong and H. Song, "Photoacoustic tomography: *in vivo* imaging from organelles to organs," *Science* **335**, 1458–1462 (2012).
27. B. Yin et al., "Fast photoacoustic imaging system based on 320-element linear transducer array," *Phys. Med. Biol.* **49**, 1339–1346 (2004).
28. S. Kothapalli et al., "Deep tissue photoacoustic imaging using a miniaturized 2-D capacitive micromachined ultrasonic transducer array," *IEEE Trans. Biomed. Eng.* **59**, 1199–1204 (2012).
29. P. Beard, "Biomedical photoacoustic imaging," *Interface Focus* **1**, 602–631 (2011).
30. A. Alex et al., "Multispectral *in vivo* three-dimensional optical coherence tomography of human skin," *J. Biomed. Opt.* **15**, 026025 (2010).

Haroon Zafar graduated with a BSc degree in electrical engineering in 2007. He was awarded with the Erasmus Mundus scholarship from European Commission in 2009 to pursue his double degree in MSc in photonics. He received his first MSc degree from UK and received a second MSc engineering degree from Belgium in 2011. He was awarded with a Hardiman research fellowship from NUI Galway in September 2011 to pursue his PhD degree in biophotonics. So far he has more than 35 journal and conference publications. He was the founding president of the NUIG-UL SPIE student chapter.

Aedán Breathnach graduated with a BSc degree in physics from the National University of Ireland (NUI), Galway. He is currently doing a PhD in biophotonics at tissue optics and microcirculation imaging facility, NUI Galway.

Hrebesh M. Subhash graduated with BS and MS degrees in applied electronics from India in 1998 and 2000, respectively. He received his MPhil degree in photonics technology from India in 2004 and received his PhD degree in technology from Yamagata University, Japan, in 2008. He is currently working as a research fellow at tissue optics and microcirculation imaging facility at NUI Galway.

Martin J. Leahy completed a DPhil at the University of Oxford and he and a colleague established Oxford Optronix Ltd., where he was director of R&D. From 1995, he had various research and teaching posts at the University of Oxford. He then joined the Stokes Research Institute, where he conducted industry-led R&D and later the Physics Department at the University of Limerick, where he led research groups in energy and biophotonics and lectured in physics. He has secured more than €7M in external R&D funding since 2003. He is an adjunct professor at the Royal College of Surgeons, fellow of the Institute of Physics in Ireland, fellow of the Royal Academy of Medicine in Ireland, and fellow of SPIE. He is currently the chair of applied physics at NUI Galway.